ARTICLE OPEN

Check for updates

PDL1-expressing macrophages infiltrate diffuse large B-cell lymphoma and promote lymphoma growth in a MYC-driven experimental model

Ningxuan Cui[1], Peter Leary[1,2], Vanesa-Sindi Ivanova[3], Kristin Stirm[1,3,4], Lydia Kirsche[1], Nicola Aceto[4], Frank Stenner[5], Lothar C. Dieterich[6], Michael Detmar[7], Ekaterina Petrova[8], Sarah Mundt[8], Melanie Greter[8], Alexandar Tzankov[3] and Anne Müller[1]✉

The infiltration of diffuse large- and other mature B-cell lymphomas with T- and myeloid cells is a key tumor microenvironmental feature but is not currently factored into treatment decisions. Here, we have used multiplex immunofluorescence microscopy to quantify the immune infiltrates of >260 diffuse large B-cell- (DLBCL), follicular- (FL) and mantle cell lymphomas (MCL), and chronic lymphocytic leukemias (CLL) relative to clinical outcomes, mutational landscape and phenotype. MCL were found to be the "coldest" and DLBCL the "hottest" entities. The lymphoma microenvironment of DLBCL featured numerically dominant populations of $CD8^+$ and T-follicular helper (Tfh) T-cells that were indicative of superior prognosis. Mutations in *EZH2*, *PTEN* and *KMT2D* were overrepresented in DLBCL with low $CD8^+$ T-cell infiltration. A unique feature of DLBCL was its infiltration by large numbers of $PDL1^+$ macrophages that constituted up to 70% of total cellularity. $PDL1^+$ macrophage infiltration was mutually exclusive with regulatory T-cell infiltration. The inducible ablation of PDL1 on macrophages was sufficient to improve immune control of MYC-expressing lymphoma in a syngeneic immunocompetent model. These results implicate the macrophage/$CD8^+$ T-cell axis as a key pathogenetic determinant and immunotherapeutic target in a subset of DLBCL patients with poor prognosis.

HIGHLIGHTS

- Multiplex IF microscopy of the lymphoma microenvironment uncovers large differences among B-cell lymphomas that are prognostically relevant.
- PDL1 expression by macrophages is a common feature of DLBCL and drives immune escape by suppressing anti-lymphoma CD8 T-cell responses.

Blood Cancer Journal (2025)15:66 ; https://doi.org/10.1038/s41408-025-01281-1

INTRODUCTION

B-cell lymphomas are genetically and clinically heterogeneous neoplasms resulting from the clonal expansion of mature B-cells arrested at various stages of differentiation. Mature B-cell lymphomas may arise at both nodal and extranodal sites, and from germinal center (GC) or post-GC B-cells. Tremendous advances have been made in exploring the genetic landscape of B-cell lymphomas using large-scale whole exome- and transcriptome sequencing as well as copy number variation analyses, which has led to the stratification of patients into characteristic genetic subtypes and supports the rationale for targeting of defined oncogenic signalling pathways [1–5]. In diffuse large B-cell lymphoma (DLBCL), at least six genetic subtypes exist: the MCD/C5 subtype features the co-occurrence of $MYD88^{L265P}$ and/or *CD79B* mutations and *BCL2* gains, the BN2/C1 subtype is characterized by *BCL6* fusions and *NOTCH2* mutations as well as genetic aberrations in numerous immune genes, e.g. *B2M*, *CD70*, *FAS*, *PDL1*, *PDL2*, the N1 subtype is assigned based on *NOTCH1* mutations, and the EZB/C3 subtype features *EZH2* mutations and *BCL2* translocations alongside inactivating mutations in the chromatin modifiers *CREBBP* and *KMT2D* [1, 4]. The C2/A53 subtype is characterized by mutations in *TP53* and copy number alterations (CNA), whereas the C4/ST2 subtype features mutations and CNA in *SGK1/SOCS1/TET2* and genes encoding for compounds of the JAK-STAT

[1]Institute of Molecular Cancer Research, University of Zürich, Zürich, Switzerland. [2]Functional Genomics Center Zürich, University of Zürich and Federal Institute of Technology Zürich, Zürich, Switzerland. [3]Institute of Medical Genetics and Pathology, University Hospital Basel, Basel, Switzerland. [4]Institute of Molecular Health Sciences, Swiss Federal Institute of Technology Zürich, Zürich, Switzerland. [5]Clinic for Medical Oncology, University Hospital Basel, Basel, Switzerland. [6]European Center for Angioscience and Mannheim Institute of Innate Immunoscience, Medical Faculty Mannheim, Heidelberg University, Heidelberg, Germany. [7]Institute of Pharmaceutical Sciences, Swiss Federal Institute of Technology Zürich, Zürich, Switzerland. [8]Institute of Experimental Immunology, University of Zürich, Zürich, Switzerland. ✉email: mueller@imcr.uzh.ch

Received: 24 March 2025 Revised: 31 March 2025 Accepted: 7 April 2025
Published online: 16 April 2025

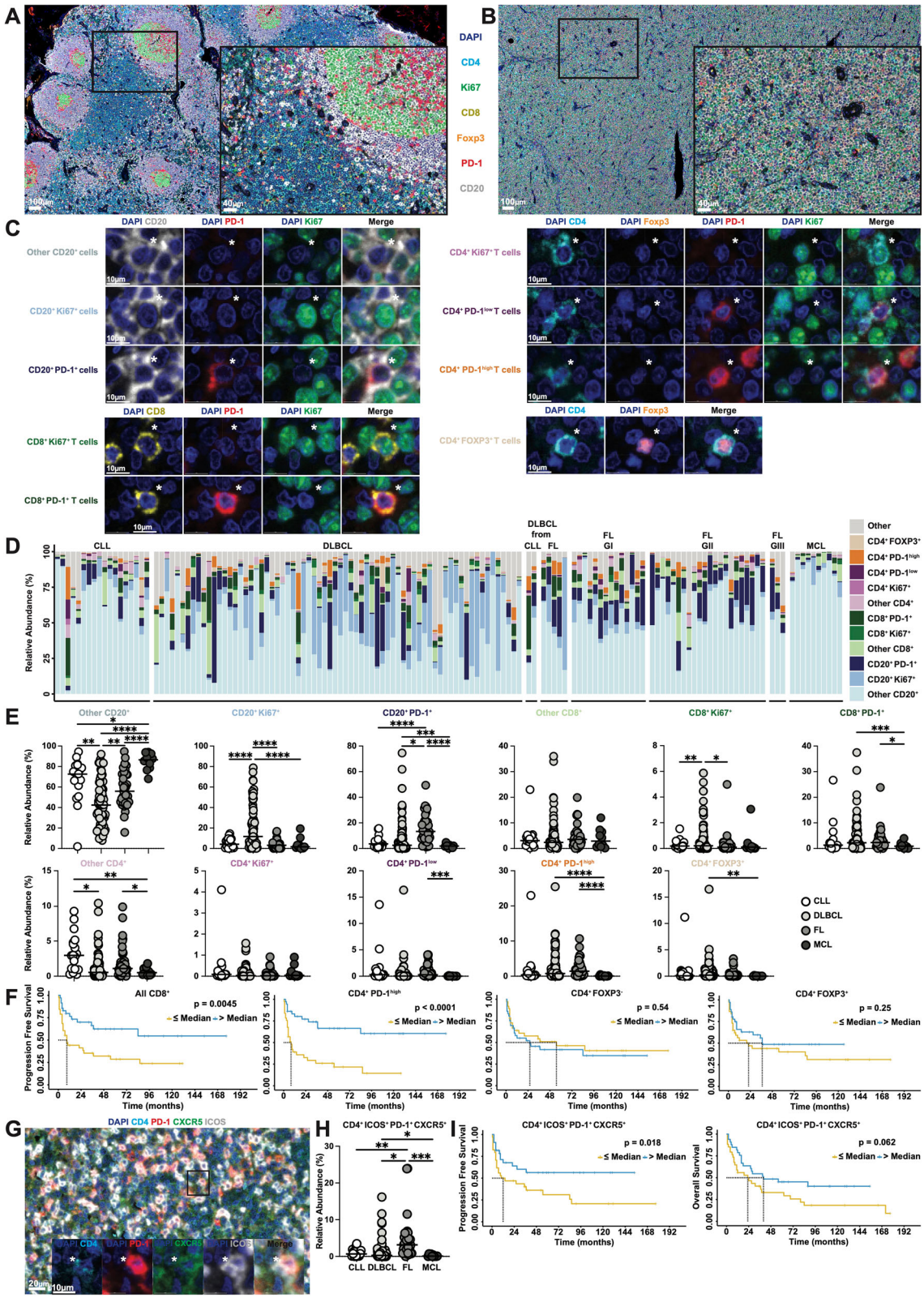

signaling [1, 4]. Moreover, the transcriptional signature of the EZH2/C3 and C4 subtypes reveals a GC B-cell-of-origin (COO) (GCB-DLBCL), the MCD/C5 and N1 subtypes' transcriptional signatures are indicative of an activated B-cell origin (ABC-DLBCL), and the COO of the C2 and BN2/C1 subtypes is less clear [1, 4]. The six subtypes further differ in their MHCII expression, which has been identified as a major immune escape mechanism not only in DLBCL but also in follicular lymphoma (FL) [6], with the EZH2/C3 and MCD/C5 subtypes exhibiting the lowest and the BN2/C1 and C2 subtype the highest MHCII expression [7].

Fig. 1 CD8$^+$ T-cells and CD4$^+$CXCR5$^+$PD1^{hi} T-follicular helper cells are overrepresented and positively prognostic in DLBCL. A–F A tissue microarray comprising 77 DLBCL, 39 FL, 10 MCL and 18 CLL cases (NHL TMA) was subjected to multiplex immunofluorescence (IF) microscopy using antibodies against CD20, CD4, CD8, PD1, Ki67 and Foxp3 (**A**) and counterstained with DAPI. Normal lymph node samples were stained with the same panel for comparison. Sections were recorded using the Vectra Polaris imaging system, and images were processed using Inform and R. Representative images of a normal lymph node, and of a representative DLBCL case are shown at low and high (inset) magnification in (**A** and **B**). A gallery of single channel and multi-channel images of the nine indicated numerically dominant tumor (CD20$^+$) and T-cell populations are shown in (**C**). Asterisks point to cells of interest. The relative abundance (in % of all cells with a DAPI$^+$ nucleus) of the populations in **C**, plus marker-negative ("other") populations, is shown in **D** in the form of stacked bar plots for all cases included in the NHL TMA (note that CD4$^+$ and CD8$^+$ populations co-expressing PD1 and Ki67 were rare and were included with "other CD4/CD8"). Patients are arrayed on the x-axis and sorted by diagnosis. The relative abundance (in % of all cells with a DAPI$^+$ nucleus) of the indicated populations as detected in the four main lymphoma entities is shown in (**E**) (note that the DLBCL cases transformed from CLL and FL are pooled here with all other DLBCL cases, and FL cases grades 1–3 are pooled into one category); each symbol represents one case. Statistical comparisons were performed by one-way ANOVA with Dunnett's T3 correction; *$p < 0.05$; **$p < 0.01$; ***$p < 0.005$; ****$p < 0.001$. Kaplan-Meier curves showing progression-free survival of the 77 patients included in the NHL TMA with large (>median) relative to small (≤median) infiltrates of CD8$^+$ T-cells, CD4$^+$ PD1^{hi} Tfh cells, CD4$^+$ Foxp3$^-$ T-cells and CD4$^+$ Foxp3$^+$ Tregs are presented in (**F**). P-values were calculated by Kaplan-Meier log-rank test. **G–I** The NHL TMA was stained using antibodies against CD4, PD1, CXCR5 and ICOS (**B**). A low magnification multi-channel image of a representative DLBCL case is shown in **G** alongside single- and multi-channel, high-magnification images (inset). The relative abundance (in % of all cells with a DAPI$^+$ nucleus) of CD4$^+$PD1$^+$CXCR5$^+$ICOS$^+$ Tfh cells in the four main lymphoma entities is shown in (**H**). Kaplan-Meier curves showing progression-free and overall survival of 77 patients included in the NHL TMA with large (>median) relative to small (≤median) infiltrates of CD4$^+$PD1$^+$CXCR5$^+$ICOS$^+$ Tfh cells are presented in (**I**). P-values were calculated by Kaplan–Meier log-rank test.

Equally heterogeneous as the genetic landscape of mutations and chromosomal aberrations, but less well understood is the cellular composition of the lymphoma microenvironment (LME). The LME composition likely governs tumor progression, treatment response and clinical outcome [8], and targeted immunotherapies interfering with LME constituents or with immune/tumor cell cross-talk in the LME are increasingly becoming available [9]. The latter include immune checkpoint inhibitors, bispecific antibodies, and chimeric antigen receptor (CAR) T-cells. Recent advances in elucidating the LME of a spectrum of lymphomas include the comprehensive single-cell-based and multimodal profiling of the FL LME, which has revealed four major FL subtypes with differential representation or relative depletion of distinct T-cell subsets [6], and stromal remodeling and extracellular matrix deposition as key features of high-risk patients [3]. In DLBCL, multiplexed ion beam imaging-time of flight (MIBI-TOF) coupled with quantitative image analysis of 51 cases has revealed three categories of LME, i.e. immune-deficient, dendritic cell–enriched, and macrophage-enriched LMEs [10].

Here, we use several complementary multiplex immunofluorescence (IF) microscopy panels to quantitatively describe the LME of >260 DLBCL, FL, mantle cell lymphoma (MCL) and chronic lymphocytic leukemia (CLL) cases (presenting as small lymphocytic lymphomas), and link specific immune cell infiltrates to treatment responses, clinical outcomes, and mutational landscapes. The results uncover substantial heterogeneity both within and across lymphoma entities and reveal specific CD8$^+$ T-cell- and T-follicular helper (Tfh) cell populations as positively, and PDL1$^+$ macrophage populations as negatively prognostic in DLBCL. The conditional and inducible ablation of PDL1 expression on murine intratumoral macrophages in a MYC-driven experimental lymphoma model confirms that these cells support lymphoma growth.

METHODS

Patient cohorts and multiplex IF microscopy

All patients have given general informed consent for their archival tissue to be used for scientific research. Construction of the TMAs was approved by the ethics committee of Northwestern and Central Switzerland (EKNZ 2014-252) for the prospectively arrayed DLBCL routine cases of the University Hospital Basel collected between 2010 and 2020 [11], and by the institutional review board of the Medical University of Innsbruck, Austria for the historic cases collected before 2001 [12]. Use of the tissue-microarrayed cases collected as part of the prospective SAKK 38/07 study (ClinicalTrials.gov NCT00544219) was approved by the Ethics Committee Beider Basel. The Opal 7-color manual IHC kit (Akoya Biosciences, cat NEL861001KT) was used for staining of TMAs; imaging of the slides was performed using the Vectra Polaris Automated Quantitative Pathology Imaging System (Akoya Biosciences). Spectrally unmixed images were generated using the inForm software package (v2.6.0; Akoya Biosciences) and further analyzed using machine learning algorithms built in the inForm software package. A detailed description of amplicon sequencing, of the antibodies used for staining, of the staining protocols and for post-processing of data is available in the supplemental methods section.

Animal experimentation

For the syngeneic serial transplantation model of MYC-overexpressing lymphoma cells harvested from *Eμ-Myc* transgenic mice [13], 1×10^6 cryopreserved splenic tumor cells in 100 µl PBS were injected intravenously into 6–8 week old mixed-gender *Mrc1*$^{Cre\text{-}ERT}$ *CD274*$^{fl/fl}$ or *Mrc1*$^{Cre\text{-}ERT}$ *Tcf7*$^{fl/fl}$ mice and their *CD274*$^{fl/fl}$ or *Tcf7*$^{fl/fl}$ littermates as described in detail previously [14]. The construction of the *Mrc1*$^{Cre\text{-}ERT}$ strain is described alongside protocols for tamoxifen application, antibody administration, and flow cytometry in the supplemental methods section. All animal studies were reviewed and approved by the Zurich Cantonal Veterinary Office (licenses 132/2019 and 007/2022 and their amendments, to A.M.).

RESULTS

The lymphoma microenvironment is highly variable across and within B-cell lymphoma entities as determined by multiplex immunofluorescence microscopy

To begin investigating the cellular composition of the LME of B-cell lymphoma, we stained a tissue microarray (TMA) comprising 70 DLBCL cases, 18 cases of CLL, 10 MCL and 39 FL (14 grade 1, 22 grade 2 and 3 grade 3) alongside 7 DLBCL cases that had transformed from CLL or FL (NHL TMA, suppl. Table 1) with a multiplex IF panel that allowed us to identify CD4$^+$ and CD8$^+$ T-cells, CD4$^+$ Foxp3$^+$ Tregs and tumor cells by their CD20 expression. Antibodies for PD1 and Ki67 were also included in the panel (panel A, suppl. Table 2) alongside the mentioned lineage markers; tumor-free, non-inflamed lymph node (LN) samples were stained in parallel as non-neoplastic controls. T- and B-cells, proliferating Ki67$^+$ B-cells and Tregs were localized in, and confined to, the T- and B-cell zones, and the germinal centers (GC) of the normal LN samples (Fig. 1A). The lymphoma samples, in contrast, exhibited a diffuse infiltrate of varying numbers of clearly discernible lymphocytic populations that were identified as CD20$^+$ tumor cells, CD4$^+$ and CD8$^+$ T-cells (each expressing either Ki67, or low levels of PD1, or neither marker), CD4$^+$ Foxp3$^+$ Tregs, and CD4$^+$ PD1^{high} cells (Fig. 1B, C, suppl. Fig. 1A). Cell segmentation and phenotyping using Inform (suppl. Fig. 1B, C), followed by post-processing of raw data in R allowed us to quantify all populations for each patient, which revealed several striking differences. MCL cases consisted mostly of tumor B-cells

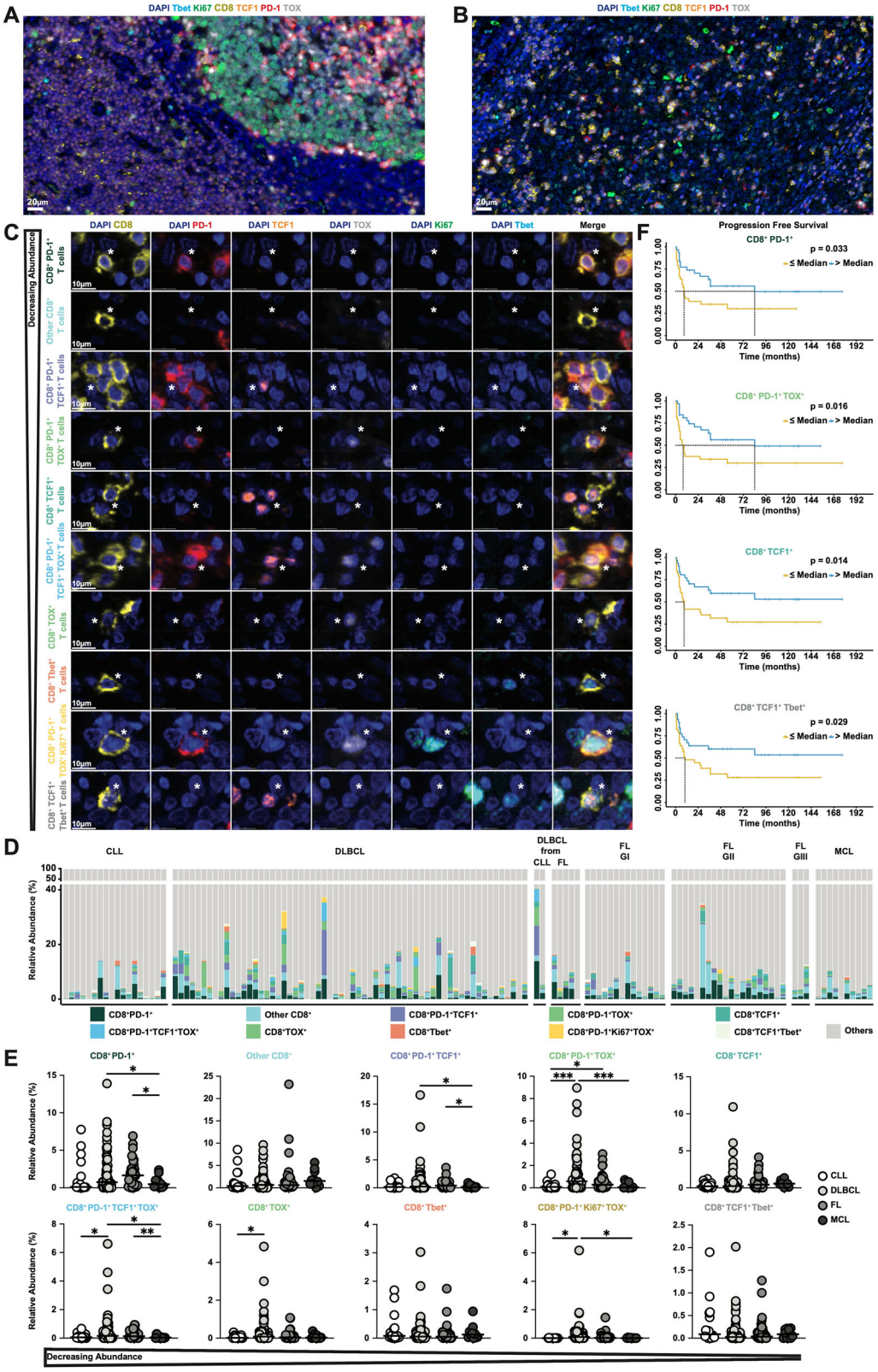

(>80% tumor content), and were comparatively "cold", i.e. featured very few non-malignant cells in the tumor mass (Fig. 1D, E). As expected, the proliferating fraction of tumor cells ($CD20^+$ $Ki67^+$) was higher in DLBCL than in the other lymphomas (Fig. 1D, E). A majority of FL and their high-grade-transformed counterparts, and a small number of primary DLBCL cases showed high levels of tumor cell-intrinsic PD1 expression ($CD20^+$ $PD1^+$) that set these cases apart from the other entities (Fig. 1D, E). $CD8^+$ T-cells constituted the numerically dominant, but highly variable lymphoma-infiltrating lymphocyte population across all

Fig. 2 Exhausted CD8$^+$ T-cells and their precursors represent specific components of the LME of DLBCL, but not of other lymphomas, and in DLBCL are associated with longer progression-free survival. A–F The NHL TMA was stained with antibodies against CD8, PD1, Ki67, TOX, TCF1 and Tbet (**C**) and counterstained with DAPI. Normal lymph node samples were stained with the same panel for comparison. Sections were recorded and processed as described in Fig. 1. Representative images of a normal lymph node, and of a representative DLBCL case are shown at high magnification in (**A**, **B**). A gallery of single channel and merged (all channels) images of the ten indicated numerically dominant tumor-infiltrating CD8$^+$ T-cell populations is shown in **C**, arranged in the order of decreasing abundance. Asterisks point to cells of interest. The relative abundance (in % of all cells with a DAPI$^+$ nucleus) of the populations in **C**, plus marker-negative ("other") populations, is shown in **D** in the form of stacked bar plots for all cases included in the TMA. Patients are arrayed on the x-axis and sorted by diagnosis. The relative abundance (in % of all cells with a DAPI$^+$ nucleus) of the indicated populations as detected in the four main lymphoma entities is shown in **E** (arranged by decreasing abundance); each symbol represents one case. Statistical comparisons were performed by one-way ANOVA with Dunnett's T3 correction; *$p < 0.05$; **$p < 0.01$; ***$p < 0.005$. Kaplan-Meier curves showing progression-free survival of patients with large (>median) relative to small (≤median) infiltrates of the indicated prognostically relevant CD8$^+$ T-cell populations are presented in (**F**). P-values were calculated by Kaplan-Meier log-rank test. Note that in **C**–**F**, markers that are negative do not feature in the population designation; for example, the population "CD8$^+$ PD1$^+$" is negative for all other markers. Please see suppl. Fig. 2 for overall survival Kaplan-Meier curves.

lymphoma entities, with a specific overrepresentation of CD8$^+$ PD1$^+$ T-cells. CD4$^+$ T-cells and Foxp3$^+$ Tregs were generally less abundant (Fig. 1D, E). CD4$^+$ PD1^{high} cells were overrepresented in DLBCL and FL relative to the other entities (Fig. 1D, E).

We next examined how the various lymphoma-infiltrating populations correlate with the clinical outcomes. The four main entities in our cohort differed strongly in terms of their disease course; patients diagnosed with FL or CLL had a much better prognosis on standard of care treatment than patients diagnosed with DLBCL or MCL (suppl. Fig. 1D). The large differences in prognosis confounded comparisons across lymphoma entities. However, within the cohort of 77 DLBCL cases for which long-term follow-up (median follow-up: 28 months) was available, the infiltration of CD8$^+$ T-cells and of CD4$^+$ PD1^{high} cells was highly prognostic of both progression-free- and overall survival on CHOP chemotherapy (Fig. 1F, suppl. Fig. 1E). In contrast, the remaining CD4$^+$ T-cells and Foxp3$^+$ Tregs were not prognostically relevant (Fig. 1F, suppl. Fig. 1E). In FL, neither the CD8$^+$ T-cell infiltrate, nor the CD4$^+$ PD1^{high} cell infiltrate was prognostically relevant (suppl. Fig. 1F). Stratification by COO using the Hans algorithm revealed that CD8$^+$ and CD4$^+$ PD1^{high} T-cells were both prognostically more important in the non-GCB/ABC than in the GCB-DLBCL subtype (suppl. Fig. 1G). Multivariate analyses taking into account the gender, age, IPI and COO confirmed that a high infiltration with CD8$^+$ and CD4$^+$ PD1^{high} T-cells was significantly positively prognostic in terms of overall and progression-free survival, independently of these well-known prognostic indicators (suppl. Fig. 1H). As the above-mentioned CD4$^+$ PD1^{high} cells had a major impact on survival, we explored this lineage further. CD4$^+$ PD1^{high} cells were CD3$^+$ but negative for the natural killer cell marker NKp46 and the mucosa-associated invariant T-cell (MAIT) cell marker CD161 (both of which were extremely rarely expressed in our cohort; suppl. Fig. 1I–K), and expressed the T-follicular helper (Tfh) cell markers CXCR5 and ICOS, firmly establishing these cells as Tfh cells (Fig. 1G). The quantification of CD4$^+$ PD1^{high} CXCR5$^+$ ICOS$^+$ Tfh cells based on a dedicated Tfh panel (panel B, using antibodies against CD4, PD1, CXCR5 and ICOS) confirmed the overrepresentation of this cell type in DLBCL and FL relative to MCL and CLL (Fig. 1H, suppl. Fig. 1L), and the association with a good prognosis in DLBCL (Fig. 1I). These data point to substantial variability, both across and within lymphoma entities, of the cellular infiltrates of the LME, and suggest that an abundant T-cell infiltrate at diagnosis is associated with a comparatively good prognosis in DLBCL.

CD8$^+$ T-cells expressing one or more exhaustion markers are positively prognostic in DLBCL

Given the overall positive prognostic impact of CD8$^+$ T-cells in DLBCL, we set out to define in more detail their surface marker and transcription factor expression profile. To this end, the NHL TMA described above was stained for CD8 and PD1, as well as the functional markers T-cell factor 1 (TCF1), thymocyte selection-associated HMG box (TOX), Ki67 and Tbet (panel C, suppl. Table 2). Antibodies to KLRG1 and perforin were used in small two-color panels alongside anti-CD8. Ki67, TOX, TCF1 and PD1 were expressed in distinct, well-organized B- and T-cell areas of the normal LN (Fig. 2A). Much more diverse and variable T-cell populations were found in the lymphomas; 10 distinct CD8$^+$ T-cell populations could be distinguished based on their marker (co-) expression and prognostic significance (Fig. 2B, C). The most abundant subpopulations of CD8$^+$ T-cells expressed PD1, TCF1 or TOX, or combinations thereof; Ki67$^+$ or Tbet$^+$ CD8$^+$ T-cells were comparatively rare (Fig. 2C–E). KLRG1 was not expressed on CD8$^+$ T-cells, which were however positive for perforin (suppl. Fig. 2A, B). PD1, TCF1 and TOX, alone and especially in their combinations, mark T-cells at various stages of exhaustion due to chronic antigen exposure, as well as their precursors [15, 16]. Such exhausted T-cells, and their stem-like precursors, were specifically over-represented in DLBCL (and to some extent in FL) relative to the other examined lymphoma entities (Fig. 2D, E). In contrast, CD8$^+$ T-cells lacking these markers or expressing only Tbet were equally abundant in all examined lymphomas (Fig. 2D, E). Interestingly, although being overrepresented in DLBCL, the CD8$^+$ T-cell populations expressing one or more exhaustion markers tended to be prognostically beneficial in DLBCL (Fig. 2F, suppl. Fig. 2C; only trends observed for overall survival). The combined data indicate that the majority of CD8$^+$ cells infiltrating DLBCL express PD1, TOX and/or TCF1, which has positive prognostic relevance in DLBCL and sets this tumor entity apart from other types of lymphoma.

T-cell infiltration differs between the genetic subtypes of DLBCL as determined by targeted amplicon sequencing

Having identified CD8$^+$ T-cells and Tfh cells as enriched in DLBCL relative to other lymphoma entities, we asked whether their distribution could be linked to specific mutational patterns. To this end, we applied our panel A (suppl. Table 2) to a TMA comprising two prospectively collected DLBCL patient cohorts ("amplicon-sequenced DLBCL TMA", suppl. Table 1), of which one was collected in the framework of the Swiss SAKK 38/07 trial, and the other during routine diagnostics at the University Hospital Basel; both had previously been subjected to targeted amplicon sequencing of the most recurrently mutated genes in this malignancy [11, 17]. Cell segmentation and phenotyping followed by post-processing of the raw data in R confirmed the differential abundance of CD8$^+$ T-cells and of CD4$^+$ PD1^{high} Tfh cells also in these two additional cohorts (Fig. 3A). The spectrum of mutations we found was similar to what has been published in other cohorts (Fig. 3A) [1, 4]. We were able to assign a genetic subtype as proposed by Schmitz et al. [1] and later amended by Pedrosa et al. [18] by applying a two-step classifier [11]; this strategy allowed the genetic classification of the majority of cases (57 of 78; Fig. 3A). Mutations affecting the *NOTCH1* gene were overrepresented, and mutations affecting the *PTEN*, *EZH2* and *KMT2D* genes were

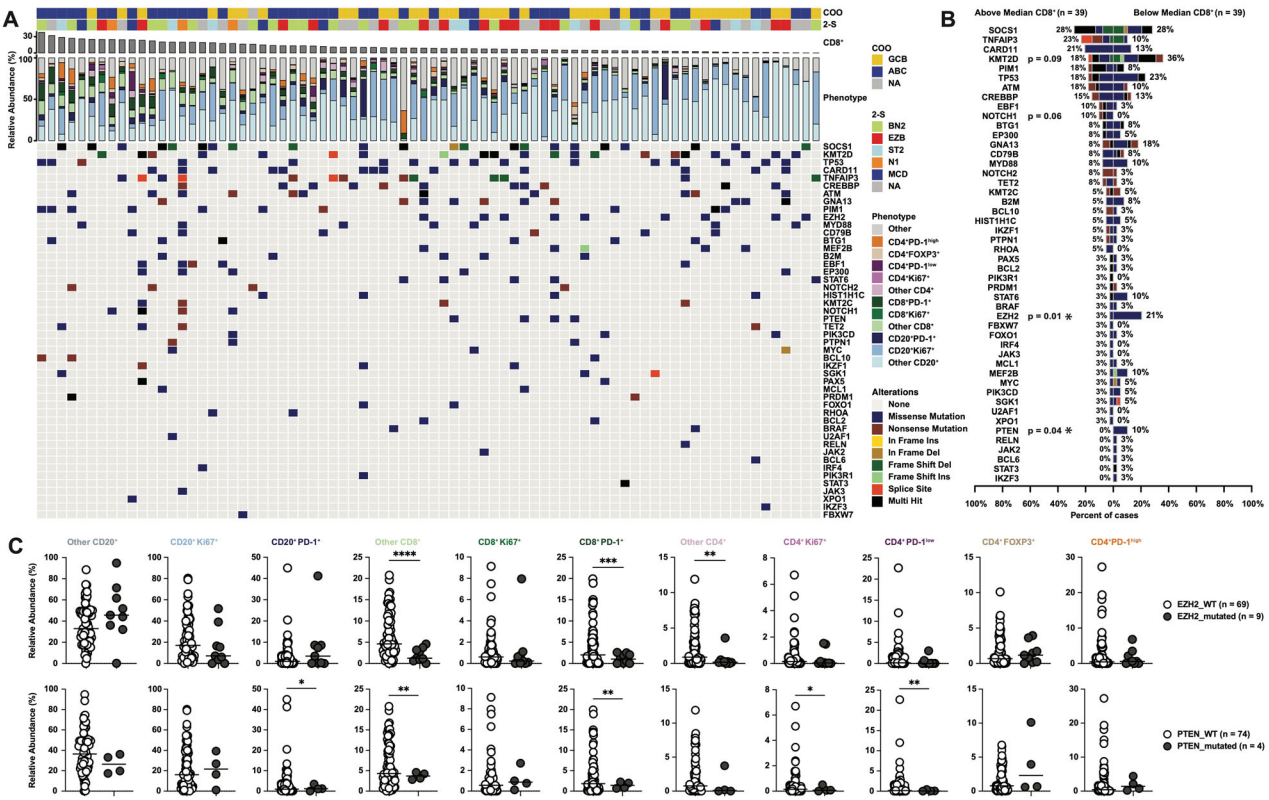

Fig. 3 Mutations in *EZH2* and *PTEN* are overrepresented in DLBCL cases with low CD8$^+$ T-cell infiltration. A–C A TMA comprising 78 amplicon-sequenced DLBCL cases ("amplicon-sequenced DLBCL" TMA) was stained with antibodies against CD20, CD4, CD8, PD1, Ki67 and Foxp3 (**A**) and DAPI. An oncoplot of the alterations occurring in at least one case (48 in total; categorized as missense, nonsense, splice site, multi-hit mutations, frame shift or in-frame deletions/insertions; most common mutations at the top, least common at the bottom) is shown in (**A**). Each case is annotated with stacked bar plots showing the relative abundance (in % of all cells with a DAPI$^+$ nucleus) of the 12 indicated tumor and T-cell populations, the cell-of-origin (COO) classification and the genetic subtype (using the 2-step classifier; 2-S). Cases are arrayed according to their CD8$^+$ T-cell infiltrate (decreasing from left to right). A co-barplot of the same 48 genetic aberrations, sorted from top to bottom by their recurrence in CD8$^+$ T-cell^{high} cases (> median) is shown in (**B**). Genetic aberrations in two genes (*EZH2*, *PTEN*) are significantly underrepresented in CD8$^+$ T-cell^{high} relative to CD8$^+$ T-cell^{low} (≤ median) cases. Genetic aberrations in two additional genes (*KMT2D*, *NOTCH1*) show a trend toward being under- and overrepresented in CD8$^+$ T-cell^{high} cases, respectively. Plots in **C** show the differential relative abundance of the indicated 11 populations (excluding the marker-negative cells) as a function of the *EZH2* (top row) and *PTEN* (bottom row) mutational status. P-values in **B** were calculated using Fisher's exact test; p-values in **C** were calculated by unpaired t-test with Welch's correction; *p < 0.05; **p < 0.01; ***p < 0.005; ****p < 0.001.

underrepresented in cases with a high CD8$^+$ T-cell infiltrate (i.e. greater than the median; two of the four genes show trends only; Fig. 3A, B). A more detailed comparison of *PTEN*- and *EZH2*-mutant cases relative to wild type cases revealed a lower infiltration of the former with both CD8$^+$ and CD4$^+$ T-cell populations (Fig. 3C). The differences in immune infiltrates between COO and genetic subtypes were overall quite modest (suppl. Fig. 3A, B). Stratification of the cases by their CD4$^+$ PD1^{high} Tfh cell infiltrates revealed that mutations affecting *BTG1*, *MYC* and *BCL2* were underrepresented in cases with a high Tfh T-cell infiltration (suppl. Fig. 3C–E). These data are in line with prior observations [19] and indicate that the presence of prognostically relevant CD8$^+$ and Tfh T-cells can at least partly be attributed to specific mutation patterns.

PDL1 expression in macrophages is a hallmark of DLBCL with poor prognosis and mutually exclusive with Treg recruitment

As CD8$^+$ T-cells and especially their PD1$^+$ exhausted subpopulations were found to be prognostically relevant and strongly overrepresented in DLBCL relative to other lymphomas, we devised a multiplex IF panel that allowed us to visualize and quantify the expression of the PD1 ligand, PDL1, and to quantify and phenotype CD68$^+$ macrophages alongside CD8$^+$ PD1$^+$ T-cells (panel D, suppl. Table 2). Panel D contained antibodies for CD8, PD1, TCF1, PDL1, CD68 and CD79a and was applied to the amplicon-sequenced DLBCL TMA, and to the NHL TMA. Whereas only very few macrophages were detected in the normal LNs, which tended to be negative for PDL1 and TCF1 (Fig. 4A), we uncovered a substantial overlap of the expression of CD68 and PDL1 in our DLBCL cases (Fig. 4B). A minority of DLBCL expressed PDL1 tumor cell-intrinsically (see a representative case in suppl. Fig. 4A). Whereas high TCF1 expression was limited to CD8$^+$ T-cells as shown above (Fig. 2), we found a subset of PDL1$^+$ macrophages that also clearly, albeit weakly, expressed TCF1 (Fig. 4B–D); this observation is in accordance with human protein atlas data, which show low level TCF1 expression in macrophages from a whole range of tissues (https://www.proteinatlas.org/ENSG00000081059-TCF7/single+cell). The abundance of macrophages and of CD8$^+$ T-cells was highly variable across cases, with ABC-DLBCL cases generally being infiltrated more extensively than GCB-DLBCL cases (Fig. 4D, E). The BN2 genetic subtype exhibited the highest PDL1$^+$ macrophage infiltration (Fig. 4F, suppl. Fig. 4B). Mutations affecting the *KMT2D* and *PIM1* genes were significantly overrepresented in cases with a high PDL1$^+$ CD68$^+$ macrophage infiltrate (i.e. greater than the median; suppl. Fig. 4C, D). Spatial analysis of the nearest cellular neighbors (residing within a radius of 10 pixels) of PDL1$^+$ macrophages revealed their close proximity to one another, and to tumor cells (Fig. 4G, suppl. Fig. 4E).

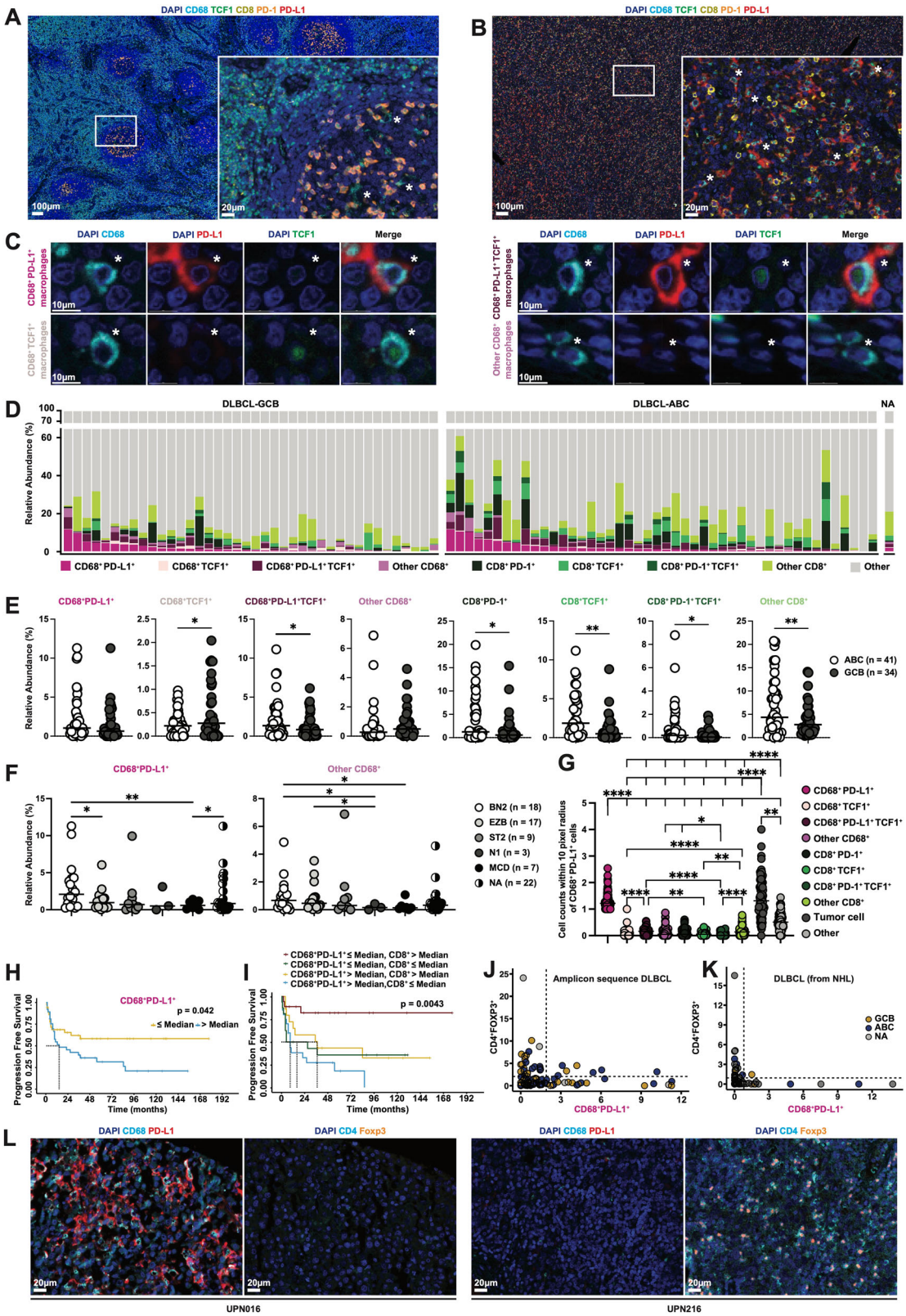

Staining of the NHL TMA with the same panel revealed that PDL1$^+$ macrophage infiltration, and especially TCF1$^+$ PDL1$^+$ macrophage infiltration, is highest in DLBCL compared to the other lymphomas (suppl. Fig. 4F), and that PDL1$^+$ macrophage infiltration is negatively prognostic in DLBCL (Fig. 4H, suppl. Fig. 4G). Patients with low PDL1$^+$ macrophage infiltration and high PD1$^+$ CD8$^+$ T-cell infiltration had the highest survival probability, and patients with high PDL1$^+$ macrophage and low CD8$^+$ T-cell infiltration had the lowest survival probability, with the other two cohorts falling in between (Fig. 4I, suppl. Fig. 4H). Both populations

Fig. 4 PDL1 expression of macrophages is associated with shorter progression-free survival and is mutually exclusive with Treg infiltration. **A**–**F** The "amplicon-sequenced DLBCL" TMA was stained with antibodies against CD8, PD1, CD68, PDL1, TCF1 and CD79a and DAPI (**D**). Normal lymph node samples were stained with the same panel for comparison. Representative images of a normal lymph node, and of a representative DLBCL case are shown at low and high (inset) magnification in (**A**, **B**) (note that the tumor/B-cell marker CD79a is not shown for the sake of clarity). A gallery of single and multi-channel images of four macrophage populations is shown in (**C**). Asterisks in **A**–**C** indicate cells of interest. The relative abundance (in % of all cells with a $DAPI^+$ nucleus) of the eight numerically dominant macrophage and $CD8^+$ T-cell populations, plus marker-negative populations ("other", also including $PDL1^+$ $CD68^-$ cells), is shown in **D** in the form of stacked bar plots for all cases included on the TMA. Patients are arrayed on the x-axis and sorted by COO classification into ABC- and GCB-DLBCL. The relative abundance (in % of all cells with a $DAPI^+$ nucleus) of the indicated populations as detected in the two COO subgroups is shown in (**E**) (macrophage populations on the left; $CD8^+$ T-cell populations on the right). The relative abundance of the indicated macrophage populations, as detected in the five genetic subtypes of DLBCL (determined using the 2-step classifier; NA not annotated), is shown in (**F**); each symbol represents one case in (**E**, **F**). Statistical comparisons in **E** and **F** were performed by one-way ANOVA with Dunnett's T3 correction; $^*p < 0.05$; $^{**}p < 0.01$. **G** Average number of cells, of the indicated populations, that reside within a 10-pixel radius of a $PDL1^+$ $CD68^+$ macrophage. Each symbol represents one of the amplicon-sequenced DLBCL patients; there are 10 dots per patient, one for each of the indicated populations. Other $PDL1^+$ $CD68^+$ macrophages, and tumor cells are the most common neighbors of $PDL1^+$ $CD68^+$ macrophages in DLBCL. **H** Kaplan-Meier curve showing progression-free survival of patients with large (>median) relative to small (<median) infiltrates of $CD68^+$ $PDL1^+$ macrophages; the cohort plotted here comprises the 77 DLBCL patients included in the NHL TMA and was stained with (**D**). **I** Kaplan-Meier curve showing progression-free survival of the same 77 DLBCL patients with > or <median infiltrates of $CD68^+$ $PDL1^+$ macrophages and $CD8^+$ T-cells. The p-values in **H** and **I** were calculated by Kaplan-Meier log-rank test. **J**, **K** Relative abundance of Tregs, vs. relative abundance of $PDL1^+$ macrophages (each in % of cells with a $DAPI^+$ nucleus), of the amplicon-sequenced DLBCL cohort (in **J**) and the NHL cohort (DLBCL patients only; **K**). The color code indicates COO. **L** Representative micrographs of sections stained for the indicated markers, of cases of which one is highly infiltrated by $PDL1^+$ macrophages but not Tregs (left panels, UPN016) and one is highly infiltrated by Tregs but not $PDL1^+$ macrophages (right panels, UPN216).

were found to be independently prognostic in multivariate analyses (suppl. Fig. 4I). Very similar survival curves were obtained when PD1 expression by $CD8^+$ T-cells was factored in (suppl. Fig. 4J). Interestingly, $PDL1^+$ macrophage infiltration was mutually exclusive with Treg infiltration, and this was observed in both DLBCL cohorts (Fig. 4J–L) upon integration of the results obtained with the staining panel used here (panel D, Fig. 4D, E) with the results from panel A. The combined data indicate that macrophages in DLBCL, but not other lymphoma entities, are programmed to express high levels of PDL1, which is negatively prognostic, especially in patients with a low ($PD1^+$) $CD8^+$ T-cell infiltrate. PDL1 expression by macrophages and Treg recruitment to the tumor mass appear to be two mutually exclusive features of DLBCL.

PDL1 is expressed on various macrophage populations in DLBCL but not in other B-cell lymphomas

Having included only one macrophage marker, CD68, in the panel D described above, we set out to capture the diversity of macrophage populations more broadly by including antibodies against CD163, CD206 and lysozyme alongside CD68 and PDL1 in an additional macrophage-centered multiplex IF panel (panel E, suppl. Table 2). This panel revealed an enormous diversity of tumor-infiltrating macrophages both within and across lymphoma entities (Fig. 5A–E, suppl. Fig. 5A). CD163 was the most universally expressed macrophage marker, followed by CD68, CD206 and lysozyme (Fig. 5A–E, suppl. Fig. 5A). Co-expression of CD163 and CD68 was common (Fig. 5B), and CD206 was typically co-expressed with CD163 (Fig. 5D). Lysozyme expression mainly identified monocytes that lacked macrophage lineage markers (suppl. Fig. 5A). All described macrophage and monocyte populations, not expressing PDL1, could be detected at low and comparable frequencies in the four examined lymphoma entities (Fig. 5A–D, suppl. Fig. 5A, left panels); in contrast, their PDL1-expressing counterparts were highly specific to DLBCL (Fig. 5A–D, suppl. Fig. 5A, right panels). PDL1 expression was a near-universal feature of macrophages infiltrating DLBCL and was largely absent in the other three examined entities (Fig. 5E). In fact, in approximately one third of the examined DLBCL cases, macrophages (both positive and negative for PDL1) made up half or more of the tumor cellularity (Fig. 5E). Cumulative PDL1 expression on any macrophage population (CD163-, CD68-, CD206-positive, alone and in combinations) set the DLBCL cases apart from the other three entities (Fig. 5F), and was negatively prognostic (Fig. 5G). Principal component analysis based on macrophage infiltrates also clearly segregated the DLBCL cases from the others (Fig. 5H). We further examined the MHCII expression on macrophages, and found that all tumor-infiltrating macrophages were MHCII-negative (suppl. Fig. 5B, C). This was in contrast to macrophages in normal LNs, which expressed high levels of MHCII (suppl. Fig. 5B, C).

To confirm the high level of $PDL1^+$ macrophage infiltration in an independent cohort of DLBCL, and to examine whether the clinical history of the patients would affect the extent of their $PDL1^+$ macrophage infiltration, we compared a recently described cohort [20] of 22 cases of post-transplant DLBCL (PT-DLBCL; of which 15 were EBV-negative, and 7 were EBV-positive) to 14 cases of DLBCL arising on a background of immunosuppression due to autoimmune disease (IS-DLBCL) and 11 cases of non-immunosuppression-related DLBCL (DLBCL, NOS (not otherwise specified; Fig. 5I, J). Several additional cases presenting with various post-transplant lymphoproliferative disorders (PTLDs) were included as well (Fig. 5I, J). Interestingly, all DLBCL cases, irrespective of their clinical history, exhibited levels of $PDL1^+$ macrophage infiltration that were comparable to one another, and also comparable to the macrophage infiltration observed in our other DLBCL cohorts (Fig. 5A–E, Fig. 4D). PTLDs presenting with plasmacytic hyperplasia (PH-PTLD) or follicular hyperplasia (FH-PTDL) had noticeably smaller infiltrates of $PDL1^+$ macrophages than any of the DLBCL cases, and also smaller infiltrates than the polymorphic PTLDs (P-PTLDs; Fig. 5I, J). The combined results suggest that $PDL1^+$ macrophages infiltrate DLBCL, but not other types of lymphoma, and express a variety of macrophage markers that are highly variable from patient to patient; $PDL1^+$ macrophage infiltration is as common in DLBCL arising on a background of immunosuppression as in cases with no such clinical history.

The genetic ablation of *Cd274* expression in macrophages activates $CD8^+$ T-cells and facilitates lymphoma immune control in a MYC-driven model

To uncover possible correlates of our human findings in an experimental syngeneic immunocompetent MYC-driven lymphoma model, we intravenously injected C57BL76 mice with MYC-expressing lymphoma cells harvested from Eμ-*MYC* donor mice [13], using protocols described in detail previously [14], and stained lymphoma-infiltrating macrophages and control LN and spleen macrophages for their PDL1 expression and quantified the cells using spectral flow cytometry. PDL1 expression was strongly

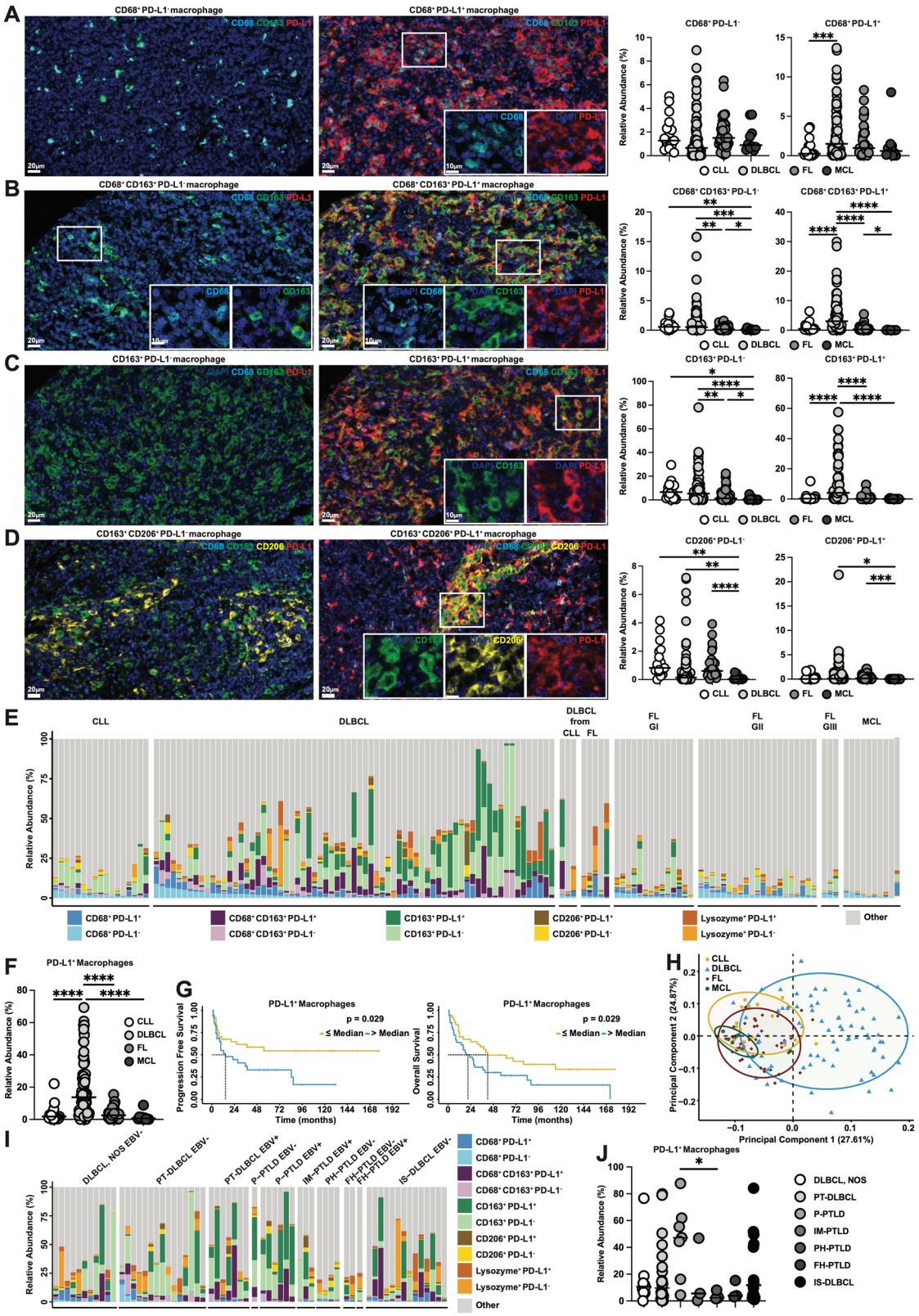

induced in F4/80-positive macrophages in the LME relative to the corresponding LNs and spleens of non-tumor-bearing control mice (Fig. 6A, B, suppl. Fig. 6A); F4/80-positive macrophage frequencies were comparable in the spleens, and elevated in the LNs of tumor-bearing relative to non-tumor-bearing mice (suppl. Fig. 6B, C). To conditionally ablate PDL1 expression specifically in macrophages, we generated a new mouse line in which Cre expression is driven by the *Mrc1* promoter (*Mrc1* encodes CD206) in a tamoxifen-inducible manner; we chose *Mrc1*/CD206 because it is highly expressed on all splenic macrophages, and a substantial

Fig. 5 PDL1 expression by a variety of macrophage populations distinguishes DLBCL from other B-cell lymphomas. A–**F** The NHL TMA was stained with antibodies against CD68, CD163, CD206, lysozyme, PDL1 and MHCII (**E**), and counterstained with DAPI. Images were recorded and processed as described in Fig. 1. Five populations of macrophages were distinguishable based on the individual or co-expression of CD68, CD163, CD206 and lysozyme; representative images of the four major populations are shown in (**A**–**D**) (see suppl. Fig. 5 for the fifth population, featuring a positive lysozyme signal). Note that all macrophages were negative for MHCII; see suppl. Fig. 5 for representative images. Each of four populations further expressed, or not, PDL1; the left and right micrograph panels in **A**–**D** show cases without (left) or with (right) PDL1 expression on the respective macrophage population. The relative abundance (in % of cells with a $DAPI^+$ nucleus) of $PDL1^-$ and $PDL1^+$ macrophage populations of all cases on the NHL TMA, stratified by lymphoma subtype, is shown in the summary plots on the right. The relative abundance (in % of cells with a $DAPI^+$ nucleus) of the five dominant macrophage populations, expressing PDL1 or not, plus marker-negative ("other") populations, is shown in **E** in the form of stacked bar plots for all cases included in the NHL TMA. Patients are arrayed on the x-axis and sorted by diagnosis. **F** The relative abundance (in % of cells with a $DAPI^+$ nucleus) of $PDL1^+$ macrophages, expressing at least one of the macrophage markers shown in (**A**–**E**), as detected in the four main lymphoma entities; each symbol represents one case. Statistical comparisons in **A**–**D** and **F** were performed by one-way ANOVA with Dunnett's T3 correction; *$p < 0.05$; **$p < 0.01$; ***$p < 0.005$; ****$p < 0.001$. **G** Kaplan-Meier curves showing progression-free (left panel) and overall (right panel) survival of 78 DLBCL patients with large (>median) relative to small (≤median) infiltrates of $PDL1^+$ macrophages expressing at least one of the markers shown in (**A**–**D**). P-values were calculated by Kaplan-Meier log-rank test. **H** PCA bi-plot showing the segregation of lymphoma entities as a function of their macrophage populations. Each symbol represents one case; patients are the same as shown in (**A**–**G**). **I**, **J** The PTLD TMA was stained with **E**, and counterstained with DAPI. The relative abundance (in % of cells with a $DAPI^+$ nucleus) of the five dominant macrophage populations, expressing PDL1 or not, plus marker-negative ("other") populations, is shown in **I** in the form of stacked bar plots for all cases included in the PTLD TMA (PTLD post-transplant lymphoproliferative disorder, NOS not otherwise specified, PT post-transplant, P polymorphic, PH plasmacytic hyperplasia, FH follicular hyperplasia, IS immunosuppression). The relative abundance (in % of cells with a $DAPI^+$ nucleus) of $PDL1^+$ macrophages, expressing at least one of the macrophage markers shown in (**A**–**E**), as detected in the five main DLBCL and PTLD entities; each symbol represents one case.

proportion of LN macrophages (suppl. Fig. 6D, E). $Mrc1^{Cre\text{-}ERT}$ mice were crossed to $Cd274^{fl/fl}$ mice (*Cd274* encodes PDL1). The resulting composite mice and their $Cd274^{fl/fl}$ littermates were intravenously injected with MYC-expressing lymphoma cells and given tamoxifen every three days to induce Cre expression. This treatment induced loss of surface PDL1 expression in splenic and LN $F4/80^+$ macrophages in Cre^+ mice but not in their Cre^- littermates (Fig. 6C, D). Interestingly, the loss of macrophage PDL1 expression significantly reduced spleen and LN weights (Fig. 6E, F) as well as the splenic and LN tumor burdens (Fig. 6G, H); tumor B-cells were distinguished from normal B-cells based on their comparatively high CD19, and low CD45 signal and their high proliferation rate (~90 of tumor B-cells are $Ki67^+$; see gating strategy in suppl. Fig. 6DF). The improved tumor control due to PDL1 loss in macrophages coincided with $CD8^+$ T-cell-, but not $CD4^+$ T-cell proliferation as determined by Ki67 staining (Fig. 6I, J, suppl. Fig. 6G, H), while the overall frequencies of $CD4^+$ and $CD8^+$ T-cells did not change (suppl. Fig. 6I, J). Interestingly, we also observed macrophage intrinsic effects of PDL1 loss, i.e. increased expression of MHCII and to a lesser extent of MHCI (Fig. 6K, L). In contrast to the effects of PDL1 ablation on macrophages, the quantitative macrophage depletion by neutralization of the growth factor receptor CSFRI failed to affect the tumor burden or T-cell activation (suppl. Fig. 6DK–P). Having observed in patients that $PDL1^+$ intratumoral macrophages are often positive for TCF1 (Fig. 4C–E), we crossed $Tcf7^{fl/fl}$ mice (*Tcf7* encodes TCF1) with the $Mrc1^{Cre\text{-}ERT}$ line described above. The inducible ablation of *Tcf7* resulted in a reduction of the splenic and LN weight and tumor burden and of PDL1 expression by intratumoral macrophages (suppl. Fig. 6DQ–X). The combined data indicate that the expression of PDL1 by macrophages in an experimental lymphoma model serves as a potent immune escape mechanism, possibly by suppressing the functionality of T-cell compartments.

CD40 activation reprograms $PDL1^+$ macrophages to upregulate antigen presentation and co-stimulation

CD40-specific agonistic antibodies have received increasing attention lately due to their ability to reprogram tumor-infiltrating myeloid cells and drive T-cell-dependent anti-tumor immunity [21, 22]. We speculated that $PDL1^+$ macrophages in our MYC-driven lymphoma model might respond to a CD40 agonist; indeed, three doses of CD40 agonist were sufficient to substantially increase the expression of MHCI, MHCII and CD80 by $F4/80^+$ intratumoral macrophages (Fig. 7A–C), and to simultaneously promote the proliferation of $CD4^+$ and $CD8^+$ T-cells in both the spleen and lymph nodes (Fig. 7D, E). The tumor burden was strongly reduced in both tissues as a consequence of the treatment (Fig. 7F, G). We asked whether CD40 was expressed on tumor-infiltrating macrophages in our MYC-driven model, and whether this cell type therefore constituted a possible direct target of CD40 activation; this was indeed the case, in particular upon the genetic ablation of PDL1 on macrophages (Fig. 7H, I). CD40 was also readily detectable on tumor-infiltrating macrophages in human DLBCL; expression of CD40 was observed in macrophages, especially if these were $PDL1^-$, and the surrounding tumor cells (Fig. 7J). The combined data indicate that CD40 activation efficiently reprograms immunosuppressive macrophages in favor of tumor control.

DISCUSSION

In this work, we used multiplex IF microscopy to comprehensively profile the LME of four major types of mature B-cell lymphomas and to correlate the relative abundance of specific lymphocytic and myeloid populations with clinical outcomes and somatic mutational landscapes. Three patient cohorts were used, of which one was from the pre-rituximab era and annotated with long clinical outcome data [12], and two were prospectively collected and annotated with targeted amplicon-sequencing data [11, 23] or a detailed clinical history (predating the lymphoma diagnosis) of the patients [20]. Although our efforts to link specific LME compartments to mutational landscapes in DLBCL were hampered to some extent by our small sample size (sequencing and immunophenotyping data were available for integration for 78 patients), we were able to identify several exciting interactions. We found *EZH2*, *PTEN* and *KMT2D* mutations to be enriched in patients with < median $CD8^+$ infiltration, which is in line with the well-documented ability of *EZH2* and *KMT2D*-mutant lymphomas to downregulate their MHCI expression, an accepted immune escape strategy [6, 24]. Equally intriguing was the finding that *BTG1* (B-cell translocation gene 1) and *MYC* mutations were both -mutually exclusively- enriched in patients with < median $CD4^+PD1^{hi}$/Tfh cell infiltration. Mutations affecting *BTG1* are drivers of DLBCL that occur in roughly 10% of cases and lower the threshold for positive selection signals from Tfh cells; *BTG1*-mutant GC B-cells experience faster cell cycle S phase transit and earlier entry into subsequent proliferative bursts [25]. Introducing the most common *BTG1* patient point mutation ($Btg1^{Q36H}$) into mice accelerates disease

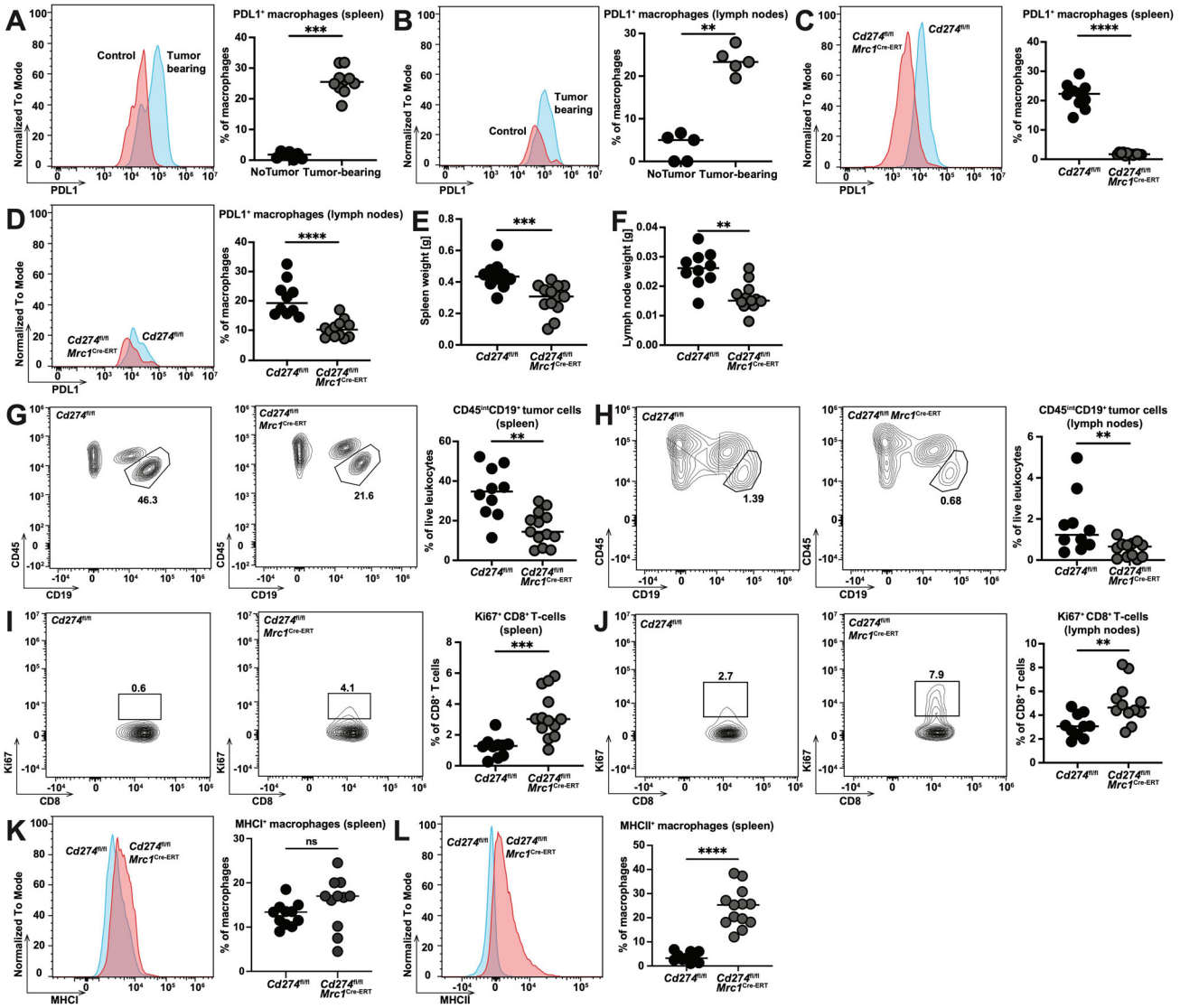

Fig. 6 The genetic ablation of PDL1 in macrophages reduces the tumor burden in a MYC-driven model of B-cell lymphoma. C57BL/6 mice were intravenously injected with 1 Mio >90% pure lymphoma cells isolated from the spleens of Eμ-*Myc*-transgenic donors; the frequencies of PDL1^{+} macrophages among all F4/80^{+} macrophages in spleen (**A**) and pooled axillary and inguinal lymph node (**B**) preparations were determined by flow cytometry at the study endpoint (10 days post injection), relative to non-tumor bearing control tissues. Representative histograms are shown alongside summary plots of one study in (**B**) and two pooled studies in (**A**). Each symbol represents one mouse. **C**–**L** *Mrc1*$^{Cre\text{-}ERT}$*Cd274*$^{fl/fl}$ mice and their *Cd274*$^{fl/fl}$ littermates were treated intraperitoneally with tamoxifen for one week prior to the intravenous transplantation of 1 Mio MYC-expressing lymphoma cells; tamoxifen administration was continued twice weekly until the study endpoint (10 days post injection). The efficiency of PDL1 ablation is shown in **C** and **D** for splenic and lymph node macrophages, respectively; representative histograms are shown alongside summary plots of two pooled studies. Spleen and lymph node weights at the study endpoint are shown in (**E**, **F**). The splenic and lymph node tumor burden, i.e. the frequency of tumor cells among all live leukocytes, is shown in (**G**, **H**). Splenic and lymph node CD8^{+} T-cell proliferation, i.e. the frequency of Ki67^{+} among all CD8^{+} T-cells is shown in (**I**, **J**). MHCI and MHCII expression by macrophages is shown in (**K**, **L**). Representative contour plots or histograms are shown alongside summary plots of two pooled studies in (**G**–**L**). p-values were calculated by unpaired two-tailed Mann-Whitney test throughout. **p < 0.01; ***p < 0.005; ****p < 0.001; n.s. not significant.

onset, shortens survival, and yields particularly invasive DLBCL-like lymphomas in a BCL2-driven lymphoma mouse model, which is due to a stronger induction of MYC-dependent growth programs [25]. Given our observation that both *BTG1* and *MYC* mutations are found in tumors with <median CD4^{+}PD1^{hi}/Tfh cells, it is tempting to speculate that such mutations provide a competitive advantage in settings of limited Tfh help. Whereas the link between *BTG1* mutations and low Tfh infiltration has not been previously established, mutations in *PTEN*, *EZH2*, *TP53* and *MYC* have been described in several other studies [8, 24]. These studies used gene set enrichment analyses of large combined genomic/transcriptomic datasets to show an association with a lower immune cell infiltration [8, 24]. While the various above-mentioned mutations were associated with lower CD8^{+} T-cell- or Tfh infiltration, we also identified a few mutations and genetic subtypes that are correlated with a T-cell-rich LME. These mostly affect NOTCH signaling (*NOTCH1/2* mutations) and the BN2/C1 and N1 genetic subtypes and have been linked previously to an inflammatory DLBCL microenvironment [1, 4].

The most striking and unexpected discovery of this study was the observation that the four examined B-cell lymphoma entities differ radically with respect to their macrophage infiltration and

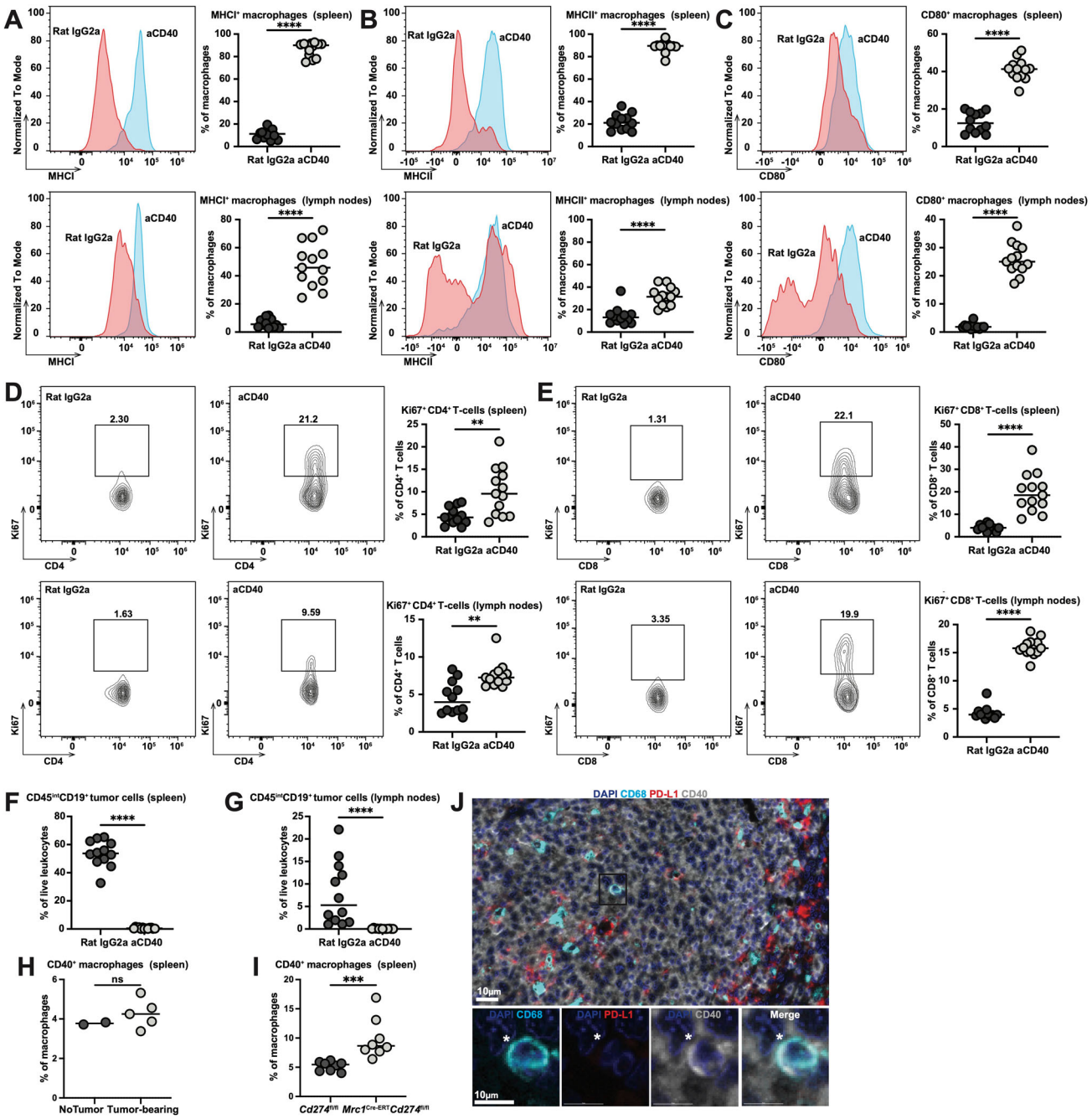

Fig. 7 A CD40 agonistic antibody reprograms intratumoral macrophages to express MHCI, MHCII and CD80, and reduces the tumor burden in a MYC-driven model of B-cell lymphoma. A–G C57BL/6 mice were intravenously injected with 1 Mio >90% pure lymphoma cells isolated from the spleens of Eμ-*Myc*-transgenic donors; mice were additionally injected with three doses of 250 μg each of CD40 agonistic, or isotype control antibody on days 0,3 and 6 days post tumor cell injection. The frequencies of MHCI$^+$, MHCII$^+$ and CD80$^+$ macrophages among all F4/80$^+$ macrophages in spleen (upper panels) and pooled axillary and inguinal LNs (lower panels) were determined by flow cytometry at the study endpoint (10 days post injection) and are shown in (**A**–**C**). The frequencies of Ki67$^+$ CD4$^+$ and Ki67$^+$ CD8$^+$ T-cells among all CD4$^+$ and CD8$^+$ T-cells in spleen (upper panels) and LNs (lower panels) are shown in (**D**, **E**), alongside representative histograms. The spleen and LN tumor burden is shown in (**F**, **G**). Each symbol represents one mouse. Two pooled studies are shown in (**A**–**G**). CD40 expression by splenic macrophages, as determined by flow cytometry, is shown for tumor-bearing and control mice in (**H**) (one study), and for tumor-bearing *Mrc1*$^{\text{Cre-ERT}}$*Cd274*$^{\text{fl/fl}}$ mice and their *Cd274*$^{\text{fl/fl}}$ littermates (treated intraperitoneally with tamoxifen) in (**I**) (two studies pooled). p-values were calculated by unpaired two-tailed Mann-Whitney test throughout. **p < 0.01; ***p < 0.005; ****p < 0.001. **J** A representative case of DLBCL was stained with antibodies against CD68, PDL1 and CD40. A low magnification multi-channel image is shown alongside single- and multi-channel, high-magnification images (inset).

the extent of macrophage PDL1 expression. Indeed, only the DLBCL cases harbored a large proportion of PDL1$^+$ macrophages. These were linked to inferior survival probability and represented abundant infiltrates in both ABC- and GCB-DLBCL; their numbers were highest in the BN2/C1 genetic subtype that is characterized by *BCL6* gene fusions and *NOTCH2* gene mutations [1, 4]. We found PDL1 expression on macrophages to be mutually exclusive with Treg infiltration, suggesting two non-redundant immune

escape mechanisms. PDL1 expression in DLBCL has been observed in 10–30% of cases (up to 80% when applying lower cut-off scores). In these cases, PDL1 is expressed tumor-cell intrinsically; this is usually caused by genetic alterations, including structural variations in the chromosomal region containing the *PDL1* and *PDL2* loci [26–29] or within the 3′ untranslated region of the *PDL1* gene [30]. In our cohorts, 10 of the 77 historical DLBCL/transformed DLBCL cases and 5 of the 78 more recently collected DLBCL cases were tumor cell-intrinsically positive for PDL1, which is in line with proportions described by others [26, 27, 31], whereas none of the FL, MCL or CLL cases were tumor-intrinsically positive for PDL1. In all our DLBCL cohorts, most non-tumor cells positive for PDL1 in DLBCL expressed at least one, and often more than one macrophage- or monocyte marker and could therefore firmly be identified as cells of myeloid origin.

To shed more light on the lymphoma macrophage compartment, we used a macrophage marker-biased panel; although small, this panel uncovered a striking level of macrophage heterogeneity both within and across the lymphoma types and even within individual tumors. CD163 was the most universally expressed macrophage marker, followed by lysozyme, CD68 and CD206; in contrast, MHCII was not expressed by intratumoral macrophages. Co-expression of CD163 with CD68 was common. While all lymphomas were infiltrated to variable extents by macrophages, DLBCL was unique in its high-level infiltration by PDL1-expressing macrophages; several extreme cases had more PDL1$^+$ macrophages than all other cells (including tumor cells) combined. These results are reminiscent of observations made in classical Hodgkin lymphoma (cHL), in which the majority of PDL1-expressing cells in the LME are in fact macrophages that typically reside close to the Reed-Sternberg cells [32]. In cHL, tumor-associated macrophages present at diagnosis are associated with treatment failure and chemoresistance [33]; the mechanism of this macrophage-driven immune evasion has been proposed to involve interactions of PDL1$^+$ macrophages with PD1$^+$ CD4$^+$ T-cells and the prevention of T-cell access to the Reed-Sternberg cells [32].

To elucidate the role PDL1$^+$ macrophages play in DLBCL, we used a MYC-driven model of B-lymphoma that shows characteristics of ABC-DLBCL [34]. In this model, the transplantation of lymphoma B-cells results in PDL1 upregulation in the macrophage compartment of lymphoid organs in which the tumor cells reside. This feature makes the model suitable for studying the consequences of macrophage PDL1 expression, although it has several limitations that preclude its application for other purposes; for example, there is no extranodal involvement, some of its features are more reminiscent of Burkitt lymphoma, and it is responsive to PD1 blockade [14], whereas relapsed/refractory DLBCL is not [35]. Indeed, the tamoxifen-inducible macrophage-specific genetic ablation of PDL1 expression activated CD8$^+$ T-cell proliferation and reduced tumor growth. These data suggest that macrophage PDL1 expression serves to dampen CD8$^+$ T-cell responses and thereby evade tumor cell killing. Interestingly, macrophage-intrinsic effects of PDL1 ablation were also observed, with macrophages expressing higher levels of MHCII upon losing PDL1; this observation points to immunosuppressive outside-in signaling through PDL1. The complete depletion of macrophages in lymphoid tissues by neutralization of CSFR1 signaling failed to phenocopy the ablation of PDL1, which is somewhat reflective of the controversial literature on macrophage infiltrate enumerations in determining DLBCL patient prognosis. In the pre-rituximab era, high numbers of tumor-infiltrating macrophages correlated with poor prognosis in DLBCL [36], while in the context of rituximab-based chemoimmunotherapy, macrophage infiltration and/or macrophage gene signatures have been associated with more favourable treatment outcomes [37, 38], and this has been attributed to a requirement for macrophages in mediating antibody-dependent cellular phagocytosis of rituximab-targeted DLBCL [39, 40]. In a small cohort of patients under CD19 CAR T-cell therapy, macrophage infiltration (defined by *CD163* and *MRC1* transcripts in scSeq data) was associated with treatment failure [41]. A recent meta-analysis summarizing data from 23 studies investigating macrophage infiltration found a significant negative association with overall, but not with progression-free survival in DLBCL patients [42], attesting to the complexity of the matter. Indeed, our data add to a growing body of evidence suggesting that the quantification of both macrophages and T-cells, using digital RNA hybridization, multiplex IF microscopy, in silico immunophenotyping or other quantitative approaches, is superior to the quantification of the single populations in predicting outcomes in DLBCL. Large T-cell infiltrates have emerged as particularly predictive of positive outcomes especially in the absence of macrophages, in both an early study that used digital RNA hybridization for CD4$^+$ and CD8$^+$ T-cell and various macrophage markers [43], and in a more recent study that used multiplex IF microscopy to the same end [44]. Our results are in agreement with these prior studies, and additionally highlight the importance of PDL1 expression by macrophages, both in patients and in an experimental lymphoma model.

In conclusion, our multiplex IF microscopy approach highlights large differences in the composition of the LME within and across lymphoma subtypes, and has both confirmed known, and revealed new genetic determinants of T-cell and macrophage infiltration. Macrophages expressing PDL1 have emerged as a numerically dominant, negatively prognostic LME compartment in DLBCL that suppresses CD8$^+$ T-cell-driven immunity in an experimental model of lymphoma.

DATA AVAILABILITY

The datasets generated and/or analysed during the current study are available from the corresponding author on reasonable request.

REFERENCES

1. Schmitz R, Wright GW, Huang DW, Johnson CA, Phelan JD, Wang JQ, et al. Genetics and pathogenesis of diffuse large B-cell lymphoma. N Engl J Med. 2018;378:1396–407.
2. Reddy A, Zhang J, Davis NS, Moffitt AB, Love CL, Waldrop A, et al. Genetic and functional drivers of diffuse large B cell lymphoma. Cell. 2017;171:481–94.e15.
3. Radtke AJ, Postovalova E, Varlamova A, Bagaev A, Sorokina M, Kudryashova O, et al. Multi-omic profiling of follicular lymphoma reveals changes in tissue architecture and enhanced stromal remodeling in high-risk patients. Cancer Cell. 2024;42:444–63.e10.
4. Chapuy B, Stewart C, Dunford AJ, Kim J, Kamburov A, Redd RA, et al. Molecular subtypes of diffuse large B cell lymphoma are associated with distinct pathogenic mechanisms and outcomes. Nat Med. 2018;24:679–90.
5. Wilson WH, Wright GW, Huang DW, Hodkinson B, Balasubramanian S, Fan Y, et al. Effect of ibrutinib with R-CHOP chemotherapy in genetic subtypes of DLBCL. Cancer Cell. 2021;39:1643–53.e3.
6. Han G, Deng Q, Marques-Piubelli ML, Dai E, Dang M, Ma MCJ, et al. Follicular lymphoma microenvironment characteristics associated with tumor cell mutations and MHC class II expression. Blood Cancer Discov. 2022;3:428–43.
7. Mondello P, Ansell SM, Nowakowski GS. Immune epigenetic crosstalk between malignant B cells and the tumor microenvironment in B cell lymphoma. Front Genet. 2022;13:826594.
8. Kline J, Godfrey J, Ansell SM. The immune landscape and response to immune checkpoint blockade therapy in lymphoma. Blood. 2020;135:523–33.
9. Laurent C, Dietrich S, Tarte K. Cell cross talk within the lymphoma tumor microenvironment: follicular lymphoma as a paradigm. Blood. 2024;143:1080–90.
10. Wright KT, Weirather JL, Jiang S, Kao KZ, Sigal Y, Giobbie-Hurder A, et al. Diffuse large B-cell lymphomas have spatially defined, tumor immune microenvironments revealed by high-parameter imaging. Blood Adv. 2023;7:4633–46.
11. Ivanova VS, Vela V, Dirnhofer S, Dobbie M, Stenner F, Knoblich J, et al. Molecular characterization and genetic subclassification comparison of diffuse large B-cell lymphoma (DLBCL)—real-life experience with 74 cases. Pathobiology. 2023;91:245–53.
12. Tzankov A, Gschwendtner A, Augustin F, Fiegl M, Obermann EC, Dirnhofer S, et al. Diffuse large B-cell lymphoma with overexpression of cyclin e substantiates poor standard treatment response and inferior outcome. Clin Cancer Res 2006;12:2125–32.

13. Adams JM, Harris AW, Pinkert CA, Corcoran LM, Alexander WS, Cory S, et al. The c-myc oncogene driven by immunoglobulin enhancers induces lymphoid malignancy in transgenic mice. Nature. 1985;318:533–8.
14. Stirm K, Leary P, Wust D, Stark D, Joller N, Karakus U, et al. Treg-selective IL-2 starvation synergizes with CD40 activation to sustain durable responses in lymphoma models. J Immunother Cancer. 2023;11:e006263.
15. Sekine T, Perez-Potti A, Nguyen S, Gorin JB, Wu VH, Gostick E, et al. TOX is expressed by exhausted and polyfunctional human effector memory CD8(+) T cells. Sci Immunol. 2020;5:eaba7918.
16. Connolly KA, Kuchroo M, Venkat A, Khatun A, Wang J, William I, et al. A reservoir of stem-like CD8(+) T cells in the tumor-draining lymph node preserves the ongoing antitumor immune response. Sci Immunol. 2021;6:eabg7836.
17. Juskevicius D, Jucker D, Klingbiel D, Mamot C, Dirnhofer S, Tzankov A. Mutations of CREBBP and SOCS1 are independent prognostic factors in diffuse large B cell lymphoma: mutational analysis of the SAKK 38/07 prospective clinical trial cohort. J Hematol Oncol. 2017;10:70.
18. Pedrosa L, Fernandez-Miranda I, Perez-Callejo D, Quero C, Rodriguez M, Martin-Acosta P, et al. Proposal and validation of a method to classify genetic subtypes of diffuse large B cell lymphoma. Sci Rep. 2021;11:1886.
19. Cerchietti L. Genetic mechanisms underlying tumor microenvironment composition and function in diffuse large B-cell lymphoma. Blood. 2024;143:1101–11.
20. Ivanova VS, Menter T, Cui N, Leary P, Zinner C, Halter JP, et al. Distinct subtypes of post-transplant lymphoproliferative disorders: CHIP-like mutations in early lesions and substantial mutational differences between EBV-positive and EBV-negative diffuse large B-cell lymphomas. Br J Haematol. 2025;206:484–504.
21. Wattenberg MM, Coho H, Herrera VM, Graham K, Stone ML, Xue Y, et al. Cancer immunotherapy via synergistic coactivation of myeloid receptors CD40 and Dectin-1. Sci Immunol. 2023;8:eadj5097.
22. Liu PS, Chen YT, Li X, Hsueh PC, Tzeng SF, Chen H, et al. CD40 signal rewires fatty acid and glutamine metabolism for stimulating macrophage anti-tumorigenic functions. Nat Immunol. 2023;24:452–62.
23. Tzankov A, Leu N, Muenst S, Juskevicius D, Klingbiel D, Mamot C, et al. Multiparameter analysis of homogeneously R-CHOP-treated diffuse large B cell lymphomas identifies CD5 and FOXP1 as relevant prognostic biomarkers: report of the prospective SAKK 38/07 study. J Hematol Oncol. 2015;8:70.
24. Ennishi D, Takata K, Beguelin W, Duns G, Mottok A, Farinha P, et al. Molecular and genetic characterization of MHC deficiency identifies EZH2 as therapeutic target for enhancing immune recognition. Cancer Discov. 2019;9:546–63.
25. Mlynarczyk C, Teater M, Pae J, Chin CR, Wang L, Arulraj T, et al. BTG1 mutation yields supercompetitive B cells primed for malignant transformation. Science. 2023;379:eabj7412.
26. Georgiou K, Chen L, Berglund M, Ren W, de Miranda NF, Lisboa S, et al. Genetic basis of PD-L1 overexpression in diffuse large B-cell lymphomas. Blood. 2016;127:3026–34.
27. Godfrey J, Tumuluru S, Bao R, Leukam M, Venkataraman G, Phillip J, et al. PD-L1 gene alterations identify a subset of diffuse large B-cell lymphoma harboring a T-cell-inflamed phenotype. Blood. 2019;133:2279–90.
28. Menter T, Bodmer-Haecki A, Dirnhofer S, Tzankov A. Evaluation of the diagnostic and prognostic value of PDL1 expression in Hodgkin and B-cell lymphomas. Hum Pathol. 2016;54:17–24.
29. Xu-Monette ZY, Xiao M, Au Q, Padmanabhan R, Xu B, Hoe N, et al. Immune profiling and quantitative analysis decipher the clinical role of immune-checkpoINT EXPRESSION IN THE TUMOR IMMUNE MICROENVIRONMEnt of DLBCL. Cancer Immunol Res. 2019;7:644–57.
30. Kataoka K, Shiraishi Y, Takeda Y, Sakata S, Matsumoto M, Nagano S, et al. Aberrant PD-L1 expression through 3'-UTR disruption in multiple cancers. Nature. 2016;534:402–6.
31. Kiyasu J, Miyoshi H, Hirata A, Arakawa F, Ichikawa A, Niino D, et al. Expression of programmed cell death ligand 1 is associated with poor overall survival in patients with diffuse large B-cell lymphoma. Blood. 2015;126:2193–201.
32. Carey CD, Gusenleitner D, Lipschitz M, Roemer MGM, Stack EC, Gjini E, et al. Topological analysis reveals a PD-L1-associated microenvironmental niche for Reed-Sternberg cells in Hodgkin lymphoma. Blood. 2017;130:2420–30.
33. Steidl C, Lee T, Shah SP, Farinha P, Han G, Nayar T, et al. Tumor-associated macrophages and survival in classic Hodgkin's lymphoma. N Engl J Med. 2010;362:875–85.
34. Stirm K, Leary P, Bertram K, Nunez NG, Wust D, Boudesco C, et al. Tumor cell-derived IL-10 promotes cell-autonomous growth and immune escape in diffuse large B-cell lymphoma. Oncoimmunology. 2021;10:2003533.
35. Ansell SM, Minnema MC, Johnson P, Timmerman JM, Armand P, Shipp MA, et al. Nivolumab for relapsed/refractory diffuse large B-cell lymphoma in patients ineligible for or having failed autologous transplantation: a single-arm, phase II study. J Clin Oncol. 2019;37:481–9.
36. Cai QC, Liao H, Lin SX, Xia Y, Wang XX, Gao Y, et al. High expression of tumor-infiltrating macrophages correlates with poor prognosis in patients with diffuse large B-cell lymphoma. Med Oncol. 2012;29:2317–22.
37. McCord R, Bolen CR, Koeppen H, Kadel EE, 3rd, Oestergaard MZ, Nielsen T, et al. PD-L1 and tumor-associated macrophages in de novo DLBCL. Blood Adv. 2019;3:531–40.
38. Riihijarvi S, Fiskvik I, Taskinen M, Vajavaara H, Tikkala M, Yri O, et al. Prognostic influence of macrophages in patients with diffuse large B-cell lymphoma: a correlative study from a Nordic phase II trial. Haematologica. 2015;100:238–45.
39. Minard-Colin V, Xiu Y, Poe JC, Horikawa M, Magro CM, Hamaguchi Y, et al. Lymphoma depletion during CD20 immunotherapy in mice is mediated by macrophage FcgammaRI, FcgammaRIII, and FcgammaRIV. Blood. 2008;112:1205–13.
40. Uchida J, Hamaguchi Y, Oliver JA, Ravetch JV, Poe JC, Haas KM, et al. The innate mononuclear phagocyte network depletes B lymphocytes through Fc receptor-dependent mechanisms during anti-CD20 antibody immunotherapy. J Exp Med. 2004;199:1659–69.
41. Yan Z, Li L, Fu D, Wu W, Qiao N, Huang Y, et al. Immunosuppressive tumor microenvironment contributes to tumor progression in diffuse large B-cell lymphoma upon anti-CD19 chimeric antigen receptor T therapy. Front Med. 2023;17:699–713.
42. Lin M, Ma S, Sun L, Qin Z. The prognostic value of tumor-associated macrophages detected by immunostaining in diffuse large B cell lymphoma: a meta-analysis. Front Oncol. 2022;12:1094400.
43. Keane C, Vari F, Hertzberg M, Cao KA, Green MR, Han E, et al. Ratios of T-cell immune effectors and checkpoint molecules as prognostic biomarkers in diffuse large B-cell lymphoma: a population-based study. Lancet Haematol. 2015;2:e445–55.
44. Autio M, Leivonen SK, Bruck O, Karjalainen-Lindsberg ML, Pellinen T, Leppa S. Clinical impact of immune cells and their spatial interactions in diffuse large B-cell lymphoma microenvironment. Clin Cancer Res. 2022;28:781–92.

ACKNOWLEDGEMENTS

The authors would like to thank all members of the Müller and Tzankov labs for helpful comments and discussions. This work was supported by the Swiss Cancer League (KFS-5228-02-2021 to AM and AT, KFS-5533-02-2022 to MG), the ETH lymphoma challenge (LC-02-22 to AM, AT and NA), the Swiss National Science foundation (Project grant 310030_192490 to AM), and the Clinical Research Priority Program "Precision Oncology" of the University of Zurich. Additional support was provided by the Forschungskredit of the University of Zurich (to KS) and the Comprehensive Cancer Center Zurich (to PL). The sponsors had no role in the study design, data analysis or any other part of the research and manuscript submission. The authors declare no competing financial interests.

AUTHOR CONTRIBUTIONS

NC designed, performed and analyzed experiments and co-wrote the manuscript. PL contributed bioinformatic analyses. LK, V-SI and KS helped with experiments. NA, SM, MG, LCD, MD and EP provided critical tools and reagents as well as advice. FS and AT provided patient samples, TMAs and access to clinical data, and AM and AT supervised the study; AM wrote the manuscript.

COMPETING INTERESTS

The authors declare no competing interests.

ETHICS

All methods were performed in accordance with the relevant guidelines and regulations.

ADDITIONAL INFORMATION

Supplementary information The online version contains supplementary material available at https://doi.org/10.1038/s41408-025-01281-1.

Correspondence and requests for materials should be addressed to Anne Müller.